Journal of Cerebral Blood Flow & Metabolism (2011) 31, 113–123

www.jcbfm.com

Quantitative analysis of [^{11}C]AZ10419369 binding to 5-HT$_{1B}$ receptors in human brain

Katarina Varnäs[1], Svante Nyberg[2], Christer Halldin[1], Andrea Varrone[1], Akihiro Takano[1], Per Karlsson[1], Jan Andersson[1], Dennis McCarthy[3], Mark Smith[3], M Edward Pierson[3], Johan Söderström[2] and Lars Farde[1,2]

[1]*Psychiatry Section, Department of Clinical Neuroscience, Karolinska Institutet, Karolinska University Hospital, Stockholm, Sweden;* [2]*AstraZeneca Pharmaceuticals Clinical Neuroscience, Södertälje, Sweden;* [3]*AstraZeneca Pharmaceuticals CNS Discovery, Wilmington, Delaware, USA*

A novel radioligand for positron emission tomography (PET) imaging of serotonin 5-HT$_{1B}$ receptors, [^{11}C]AZ10419369, has been recently described. In this study, the potential for quantitative analysis of [^{11}C]AZ10419369 binding to central 5-HT$_{1B}$ receptors was evaluated in human subjects. PET measurements were performed after injection of [^{11}C]AZ10419369 in 10 subjects. Data were analyzed with kinetic modeling and linear graphical analysis using the arterial plasma as input function, and with reference tissue models using cerebellar cortex as the reference region. Binding of [^{11}C]AZ10419369 was highest in pallidum, ventral striatum, and occipital cortex and lowest in cerebellum. The percentage of unchanged radioligand in plasma was 97% to 99%, indicating that no significant amounts of radioactive metabolites were formed during the time of analysis. Time–activity curves of [^{11}C]AZ10419369 could be described with both one-tissue compartment (1-TC) and two-tissue compartment (2-TC) models in the majority of subjects. The 2-TC model failed to deliver reasonable estimates of the kinetic parameters. However, stable estimates of binding potential (BP_{ND}) were obtained by constraining K_1/k_2 to the distribution volume obtained with the 1-TC model in the cerebellar cortex. BP_{ND} values estimated with reference tissue models were correlated with the corresponding values obtained with kinetic modeling. The findings support the use of reference tissue models in applied clinical studies with [^{11}C]AZ10419369.
Journal of Cerebral Blood Flow & Metabolism (2011) **31,** 113–123; doi:10.1038/jcbfm.2010.55; published online 28 April 2010

Keywords: brain imaging; 5-HT; kinetic modeling; positron emission tomography; receptor imaging

Introduction

The brain serotonin (5-HT) system is involved in a variety of physiologic functions and is an important target in the pharmacologic treatment of neuropsychiatric disorders (Barnes and Sharp, 1999; Gingrich and Hen, 2001). The 5-HT$_{1B}$ receptor subtype is 1 of 14 known 5-HT receptors (Hoyer *et al*, 2002) and has received attention for its potential implication in the pathophysiology and treatment of depression (for a review, see Ruf and Bhagwagar, 2009), substance abuse (Crabbe *et al*, 1996; Rocha *et al*, 1998), and anxiety disorders (Lin and Parsons, 2002).

Correspondence: Dr K Varnäs, Psychiatry Section, Department of Clinical Neuroscience, Karolinska Institutet, R5:02, Karolinska University Hospital, SE-17176 Stockholm, Sweden.
E-mail: Katarina.Varnas@ki.se
The work at Karolinska Institutet was supported by a grant from AstraZeneca and the Swedish Science Council (VR 09114). Parts of the data have been presented at the Neuroreceptor Mapping Symposium in Pittsburgh, July 2008.
Received 30 January 2010; revised 19 March 2010; accepted 23 March 2010; published online 28 April 2010

The 5-HT$_{1B}$ receptor is predominantly localized in axon terminals (Sari *et al*, 1999), and has been shown to inhibit synaptic release of serotonin and other neurotransmitters (Engel *et al*, 1986; Maura and Raiteri, 1986; Sarhan *et al*, 2000). In line with a crucial role in the regulation of neurotransmitter levels, findings from animal research suggest the involvement of this receptor subtype in the control of a variety of behaviors, such as feeding (Lee and Simansky, 1997), locomotion (Ramboz *et al*, 1996), learning and memory (Åhlander-Lüttgen *et al*, 2003; Malleret *et al*, 1999), impulse control, and aggression (Ramboz *et al*, 1996; Saudou *et al*, 1994). Until recently, research on the functional role of the human brain 5-HT$_{1B}$ receptor has, however, been hampered by the limited availability of tools for direct measurement of 5-HT$_{1B}$ receptor levels *in vivo*.

Recently, two 5-HT$_{1B}$ receptor radioligands, [^{11}C]AZ10419369 (Pierson *et al*, 2008) and [^{11}C]P943 (Gallezot *et al*, 2010), have been presented. AZ10419369 (5-methyl-8-(4-methyl-piperazin-1-yl)-4-oxo-4H-chromene-2-carboxylic acid (4-morpholin-4-yl-phenyl)-amide) is a selective 5-HT$_{1B}$ receptor ligand with high *in vitro* affinities for guinea pig

and human recombinant receptors ($K_D = 0.38$ and 0.37 nmol/L, respectively) and guinea pig striatum ($K_D = 1.9$ nmol/L; Maier *et al*, 2009). AZ10419369 has been recently labeled with ^{11}C and characterized as a positron emission tomography (PET) radioligand for selective visualization of 5-HT$_{1B}$ receptors in the brain of cynomolgus macaques (Pierson *et al*, 2008). It was shown that [^{11}C]AZ10419369 enters the macaque brain rapidly and to a high extent with a regional distribution in accordance with the localization of 5-HT$_{1B}$ receptors reported in autoradiographic studies (Bonaventure *et al*, 1997; Varnäs *et al*, 2001). In addition, preliminary PET measurements in two human subjects confirmed high concentrations of [^{11}C]AZ10419369 in the brain and a regional brain distribution consistent with that seen in macaques (Pierson *et al*, 2008). In this study, we report the quantitative evaluation of [^{11}C]AZ10419369 binding to human brain 5-HT$_{1B}$ receptors.

The aim of this study was to evaluate the potential for quantitative analysis of [^{11}C]AZ10419369 binding to central 5-HT$_{1B}$ receptors in human subjects. The *in vivo* characteristics of [^{11}C]AZ10419369 were analyzed with kinetic modeling using one-tissue compartment (1-TC) and two-tissue compartment (2-TC) models and linear graphical analyses with the arterial plasma as input function. In addition, binding potential (BP_{ND}, k_3/k_4; Innis *et al*, 2007) values were obtained with reference tissue models using the cerebellar cortex as reference region (Lammertsma and Hume, 1996). BP_{ND} values obtained with the different models were compared for cross-validation purposes and for selection of the most appropriate method for future quantitative applied studies with [^{11}C]AZ10419369.

Materials and methods

Radiochemistry

[^{11}C]AZ10419369 was prepared at the Karolinska Institutet by *N*-methylation of the desmethyl precursor (8-(1-piperazinyl)-5-methylchrom-2-en-4-one-2-(4-morpholinophenyl) carboxamide, obtained from AstraZeneca R&D, Wilmington, DE, USA), using carbon-11 methyl triflate, as described earlier (Pierson *et al*, 2008). The radioactivity injected ranged from 299 to 339 MBq. The specific radioactivities of the radioligand injected varied between 3,680 and 21,768 Ci/mmol, corresponding to an injected mass of 0.18 to 1.03 μg.

Subjects

The study was approved by the Medical Products Agency and by the independent Institutional Review Board/Research Ethics Committee at Karolinska Institutet, and the Radiation Safety Committee of the Karolinska University Hospital. The study was performed in accordance with the ethical principles of the Declaration of Helsinki and that are consistent with ICH (The International Conference on Harmonization)/Good Clinical Practice and applicable regulatory requirements and the AstraZeneca policy on Bioethics. Informed consent was obtained from all subjects before initiation of the study.

Enrollment procedures were carried out at AstraZeneca Clinical Unit at Karolinska University Hospital, Huddinge, and subsequent magnetic resonance imaging and PET examinations were performed at Karolinska University Hospital, Solna. Ten healthy men, aged between 21 and 34 years, underwent PET examinations with [^{11}C]AZ10419369. The subjects were healthy according to medical history, physical examination, blood and urine screening analyses, and magnetic resonance imaging of the brain.

Magnetic Resonance Imaging

Brain magnetic resonance imaging was performed in a 1.5-T General Electrics Signa (GE, Milwaukee, WI, USA) system. Two examinations were made in one session during 15 minutes. The first was T2 weighted for clinical evaluation regarding pathology. The second was T1 weighted for coregistration with PET and delineation of anatomic brain regions. The T1 sequence was a 3D spoiled gradient recalled (SPGR) protocol with the following settings: TR 23 milliseconds; TE 4 milliseconds; flip angle 50°; field of view $260 \times 180 \times 156$; matrix $256 \times 192 \times 156$; 156 mm $\times$ 1.0 mm slices; 1 NEX 8 minutes 45 seconds. The sequence was optimized for trade-off between a minimum of scanning time and a maximum of spatial resolution and contrast between gray and white matter.

Positron Emission Tomography Procedures

Individualized plaster helmets were made for each subject and used with a head fixation system in PET studies. The subject was placed recumbent with his head in the PET system. A cannula was inserted into the left or right cubital vein and another cannula into the brachial artery on the opposite side. A sterile physiologic phosphate buffer (pH 7.4) solution containing [^{11}C]AZ10419369 was injected as a bolus during 2 seconds into the cubital vein. The cannula was then immediately flushed with 10 mL saline. Brain radioactivity was measured in a consecutive series of time frames for up to 93 minutes. The frame sequence consisted of nine 20-second frames, three 1-minute frames, three 3-minute frames, and thirteen 6-minute frames.

The PET system used was Siemens ECAT EXACT HR (Knoxville, TN, USA). All acquisitions were acquired in 3D mode (Wienhard *et al*, 1994). A three-ring detector block architecture gives a 15-cm-wide field of view. The transversal resolution in the reconstructed image is about 3.8 mm full-width at half-maximum and the axial resolution is 3.125 mm. The attenuation correction of the data was obtained with the three rotating ^{68}Ge rod sources. Raw PET data were then reconstructed using the standard filtered back projection consisting of the following reconstruction parameters: 2 mm Hanning Filter, scatter correction, and a 128×128 matrix size (Wienhard *et al*, 1994).

Arterial Blood Sampling

To obtain the arterial input function, an automated blood sampling system was used during the first 5 minutes of

each PET experiment (Eriksson *et al*, 1988). Thereafter, arterial blood samples (2 mL) were taken manually at the midpoint of each frame until the end of the measurement (Farde *et al*, 1989). One milliliter of the manually drawn samples was immediately measured for 10 seconds in a well counter. After centrifugation, 0.2 mL plasma was pipetted and plasma radioactivity was measured in a well counter.

Determination of Radioactive Metabolites in Plasma

The fraction of plasma radioactivity corresponding to unchanged [^{11}C]AZ10419369 was determined as described earlier for other radioligands (Halldin *et al*, 1995). Briefly, arterial plasma samples of 2 mL, sampled at 4, 10, 20, 30, 40, 50, and 60 minutes after injection, were deproteinized with acetonitrile and analyzed by gradient high-performance liquid chromatography with radio detection (Halldin *et al*, 1995).

Regions of Interests

Before delineation of regions of interests (ROIs), the orientation of the brain was spatially normalized by having the high-resolution T1-weighted magnetic resonance images reoriented according to the line defined by the anterior and posterior commissures being parallel to the horizontal plane and the interhemispheric plane being parallel to the sagittal plane. The PET images were coregistered to the high-resolution T1-weighted magnetic resonance images into the same space using SPM2 (Wellcome Department of Imaging Neuroscience, London, UK).

Regions of interests were outlined based on the previously reported distribution pattern of 5-HT$_{1B}$ receptors in the human postmortem brain (Bonaventure *et al*, 1997; Varnäs *et al*, 2001). The delineations of anatomic brain regions were made manually on the reoriented magnetic resonance images using an in-house image analysis software, Human Brain Atlas (Roland *et al*, 1994). Regions of interests for the caudate nucleus, putamen, pallidum, and thalamus were delineated in the horizontal projection according to the criteria defined by Svarer *et al* (2005). The ventral striatum was defined on the coronal projection as described by Mawlawi *et al* (2001). Regions of interests for the prefrontal and temporal cortices were defined in 10 coronal slices and the occipital cortex ROI was delineated in 10 sagittal slices. For the cerebellar cortex, the ROIs were made on a horizontal projection on the six central slices. The ROIs were shown on the corresponding PET images and pooled for each anatomic region. The radioactivity concentration in each brain ROI was calculated for each sequential frame, corrected for radioactive decay, and plotted versus time.

Blood and Plasma Time–Activity Curves

Arterial blood data from the manual samplings were interpolated to obtain curves with one data point per second up to the end of PET acquisition. The interpolation was performed using a weighted curve fit with a smoothing factor of 100%. Blood time–activity curves were generated by connecting the automated blood sampling system curve with the interpolated curve from manual blood samples. To obtain plasma time–activity curves, the connected blood curves were multiplied with average plasma/blood ratios calculated from manual blood samples.

Data Analysis

For estimation of regional BP_{ND} values, kinetic 1-TC and 2-TC models (Huang *et al*, 1986; Mintun *et al*, 1984; Wong *et al*, 1986) and Logan linear graphical analysis (Logan *et al*, 1990) of [^{11}C]AZ10419369 data were performed with the arterial plasma as input function. In addition, BP_{ND} values were obtained independent of arterial data using the Logan noninvasive linear graphic method (Logan *et al*, 1996) and the simplified reference tissue model (SRTM; Lammertsma and Hume, 1996). The outcomes of the models were compared to select the most appropriate method for quantitative studies with [^{11}C]AZ10419369. PMOD v. 2.9 was used for all quantitative analyses.

Kinetic Compartment Analysis: The time–activity curves for [^{11}C]AZ10419369 were corrected for the effect of the remaining radioactivity in blood by subtracting radioactivity concentrations derived from arterial blood measurements assuming that the cerebral blood volume is 5% of the total brain volume (Farde *et al*, 1989; Leenders *et al*, 1990).

To derive estimates of the total distribution volume (V_T) and BP_{ND} rate constants (K_1, k_2, k_3, and k_4) in 1-TC and 2-TC models (Innis *et al*, 2007) were subsequently estimated by nonlinear least-squares curve fitting. Radioactivity in plasma was used as the arterial input function (Farde *et al*, 1989).

To improve the stability of the curve fitting, a variant of the 2-TC model was used under the assumption that nondisplaceable distribution volume is similar between the regions. In this model, the K_1/k_2 ratio in the target ROIs was fixed to the V_T value estimated using the 1-TC model in the reference region. To distinguish between the unconstrained 2-TC model and the model variant with fixed K_1/k_2 ratio, the models are referred to as 2-TC(1) and 2-TC(2), respectively.

Linear Graphical Analysis: [^{11}C]AZ10419369 binding was also analyzed using the Logan linear graphical analysis developed for reversible ligand binding (Logan *et al*, 1990). Radioactivity of [^{11}C]AZ10419369 in arterial plasma was used as the input function (Farde *et al*, 1989). The regional V_T values were calculated from the slope of the linear phase of the obtained plots and the BP_{ND} was calculated using the following equation

$$BP_{ND} = \frac{V_{T(ROI)}}{V_{T(reference)}} - 1, \quad (1)$$

where $V_{T(ROI)}$ is the distribution volume of a target region, and $V_{T(reference)}$ the distribution volume in a reference region devoid of specific binding sites. The cerebellar cortex is a region of negligible density of 5-HT$_{1B}$ receptors in the

human brain postmortem (Varnäs *et al*, 2001), and was proposed to be a suitable reference region for the estimation of free and nonspecifically bound radioligand.

BP_{ND} values were also calculated from the distribution volume ratios obtained with the Logan noninvasive model (Logan *et al*, 1996), according to the following equation:

$$BP_{ND} = DVR - 1, \quad (2)$$

where *DVR*, the distribution volume ratio, corresponds to the ratios of V_T obtained in a target region to V_T obtained in the reference region.

Simplified Reference Tissue Model: BP_{ND} values were also estimated with the SRTM (Lammertsma and Hume, 1996), which is applied under the assumption that the nonspecific volume of distribution is similar in the target and reference region, and that radioligand kinetics in the reference region can be described by the 1-TC model. In this model, radioligand in the target region is approximated to a single compartment and the estimated parameters are reduced to three: R_1 (delivery relative to the reference tissue), k_2, and BP_{ND} (Lammertsma and Hume, 1996).

Effect of Positron Emission Tomography Measurement Duration on Parameter Estimates: The time stability of V_T and BP_{ND} estimates was evaluated by analyzing time–activity curves of shorter duration (87, 81, 75, 69, 63, 57, 51, 45, and 39 minutes). The truncated time–activity curves were used to estimate regional V_T values using kinetic 1-TC and 2-TC(2) models, and BP_{ND} values using the 2-TC(2) model and the SRTM. Analysis of data for cortical and striatal regions was based on the pooled averages of binding parameters obtained in cortical and striatal subregions, respectively. For each subject, brain region and duration parameter values were expressed relative to the corresponding 93-minutes value. For each brain region and duration, the mean and s.d. over subjects was subsequently calculated. The criteria for stability of parameter estimates were defined as a mean value within 10% of the 93-minutes estimate and s.d. < 10%.

Statistical Analysis: The Akaike information criterion (Akaike, 1974) and F statistics were used to compare the outcome of the compartment model analyses. Pearson's *r* and linear regression analysis were used to analyze correlations and the relationships between estimates of V_T and BP_{ND}, respectively, obtained with the different approaches.

Results

Radioactivity in plasma reached a peak shortly after injection of [^{11}C]AZ10419369. After a rapid decrease during the initial 5 minutes of measurement, radioactivity in plasma slowly declined throughout the PET measurement. The standardized uptake value corresponding to the mean concentration of radioactivity in plasma, normalized for injected radioactivity and body weight, was 1.6 at the end of the 90-minutes measurement. There was a high inter-individual variability in plasma radioactivity concentrations, with standardized uptake value ranging from 0.42 to 3.7 at the end of the acquisition. The blood/plasma ratio showed no evidence for time-dependent variation. The mean (s.d.) values of blood/plasma ratios measured at 3, 30, and 90 minutes after injection were 0.72 (0.12), 0.68 (0.09), and 0.75 (0.20), respectively. The percentage of unchanged radioligand in plasma was between 97% and 99%, indicating that no significant amounts of radioactive metabolites were formed during the time of analysis. Figure 1A shows a representative time–activity curve for plasma and cerebellar cortex in one of the subjects (subject C). Blood and plasma radioactivity for another subject (subject D) showed a trend of increasing concentrations toward the end of the measurement (Figure 1B). The divergent shape of the blood time–activity curve was confirmed by image-derived carotid artery radioactivity data from this subject (Figure 1B, inset). This was, however, not reflected in the corresponding cerebellar cortex time–activity curve (Figure 1B).

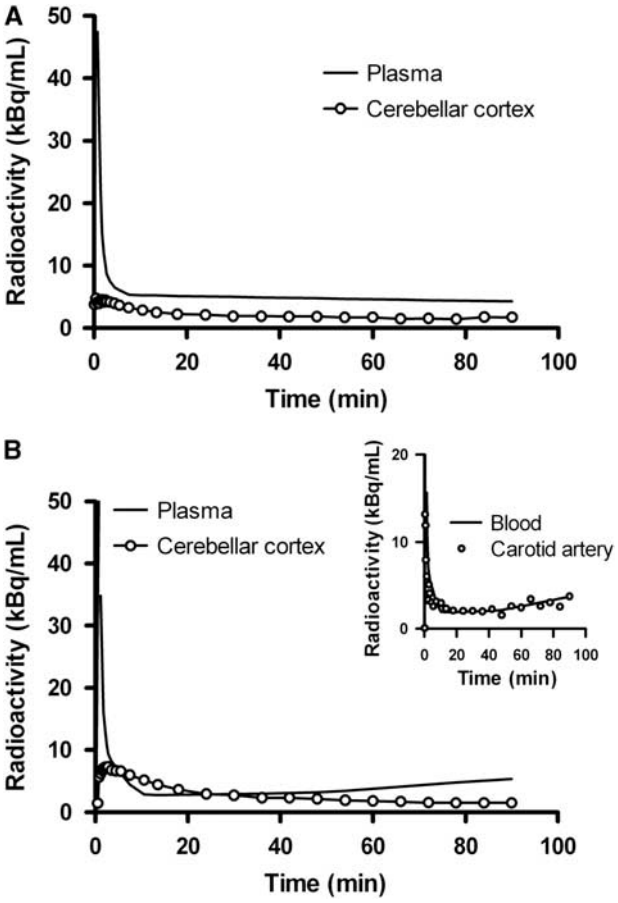

Figure 1 Radioactivity in plasma and cerebellar cortex for subject C (**A**) and subject D (**B**). Cerebellar cortex time–activity curves were corrected for intravascular activity. Inset: Blood and image-derived carotid artery radioactivity from subject D.

There was a rapid increase in brain radioactivity after intravenous injection of [^{11}C]AZ10419369, with standardized uptake value ranging from 1.1 to 2.1 at

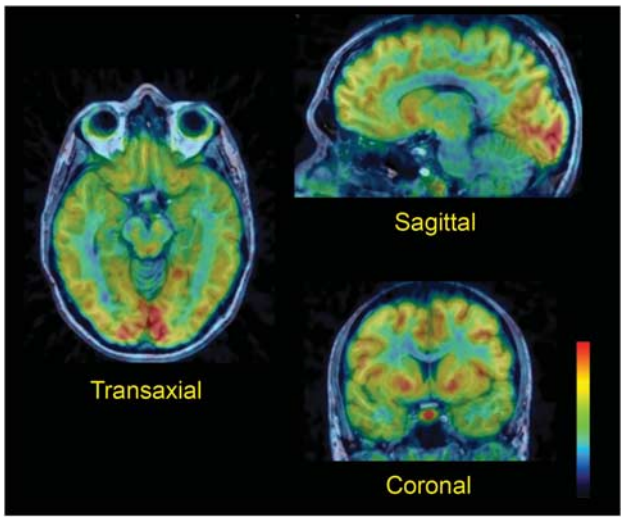

Figure 2 Fused magnetic resonance and positron emission tomography images of [^{11}C]AZ10419369 brain distribution in subject E. Images were obtained by summation of the frames from 3 to 93 minutes after intravenous injection.

the time of peak radioactivity concentration. The highest concentration of radioactivity was observed in the pallidum, the ventral striatum, and the medial occipital cortex (Figure 2). More moderate concentrations were found in other cortical regions and in the dorsal striatum, whereas radioactivity was lowest in the thalamus, pons, and cerebellum.

The brain distribution of [^{11}C]AZ10419369 was confirmed by curves for regional radioactivity versus time (Figure 3A). After an initial early peak, radioactivity slowly declined from most of the targeted regions. A different pattern with slower radioligand delivery was, however, observed in the pallidum. In this region radioactivity was initially lower as compared with other regions, and increased throughout the time of PET acquisition.

The cerebellar cortex showed the lowest radioactivity concentration among the regions analyzed and was evaluated as a reference region for nondisplaceable radioligand concentration. Radioactivity in the cerebellar cortex reached a peak within 0.5 to 1.2 minutes, with the exception for subject D (2.5 minutes), after which point it rapidly declined in this region. To describe the change in specifically bound [^{11}C]AZ10419369 over time, the curves for radioactivity in target regions minus radioactivity in the cerebellar cortex were plotted (Figure 3B). Specific binding reached maximum values in all regions, except for the pallidum, indicating that transient equilibrium was reached during the time of acquisition for other regions.

As a first step of the kinetic modeling analysis, the 1-TC and 2-TC(1) models were fitted for each region. Radioactivity concentration in the cerebellar cortex could be described by both 1-TC and 2-TC(1) models. The Akaike information criterion and the *F*-test gave no support in favor of the 2-TC(1) model. The

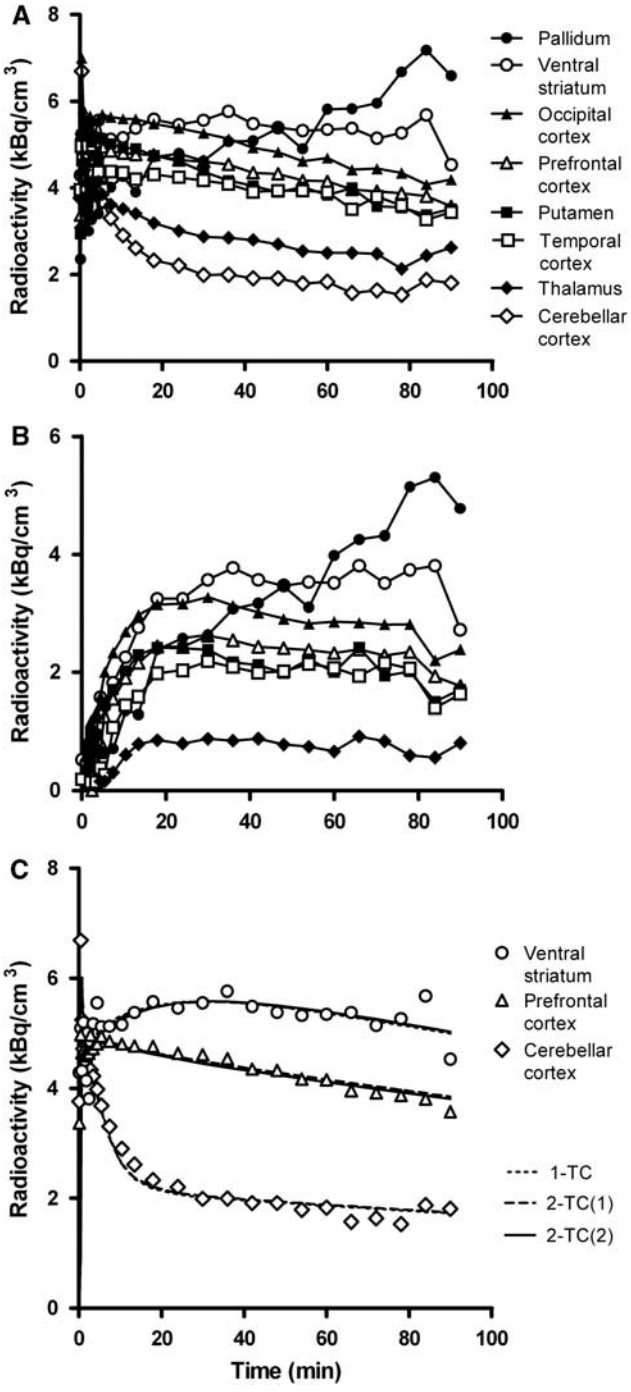

Figure 3 Time curves of brain radioactivity after intravenous injection of [^{11}C]AZ10419369 in subject C. (**A**) Regional radioactivity. (**B**) Specific binding. (**C**) Experimental values for ventral striatum, prefrontal cortex, and cerebellar cortex with the corresponding fitted curves as obtained by the one-tissue compartment model (1-TC), the unconstrained two-tissue compartment model (2-TC(1)), and the two-tissue compartment model with the K_1/k_2 ratio given by that of the cerebellar cortex (2-TC(2)).

1-TC model was thus sufficient for describing [^{11}C]AZ10419369 kinetics in 8 out of 10 subjects in the cerebellar cortex (see Supplementary Table S1 in Supplementary Information). For two of the subjects

Table 1 Comparison of the one- and two-tissue compartment models for description of [^{11}C]AZ10419369 binding in the prefrontal cortex of 10 control subjects

Subject	*Model*	K_1 *(mL/cm^3 per minute)*	k_2 *(per minute)*	k_3 *(per minute)*	k_4 *(per minute)*	k_3/k_4 *(BP_{ND})*	*SS*	*AIC*
A	1-TC	0.05	0.04	—	—	—	32	163
	2-TC(1)	0.06	0.06	0.03	0.07	0.44	31	166
	2-TC(2)	0.06	0.11	0.21	0.15	1.37	31	164
B	1-TC	0.06	0.08	—	—	—	36	177
	2-TC(1)	0.06	0.08	0.00	1.46	0.00	36	181
	2-TC(2)	0.06	0.16	3.34	3.32	1.00	36	179
C	1-TC	0.07	0.08	—	—	—	28	183
	2-TC(1)	0.07	0.08	0.00	1.45	0.00	28	187
	2-TC(2)	0.08	0.20	1.10	0.87	1.27	28	185
D	1-TC	0.13	0.10	—	—	—	49	184
	2-TC(1)	0.13	0.09	0.00	0.06	0.00	50	188
	2-TC(2)	0.14	0.19	0.68	0.78	0.87	49	186
E	1-TC	0.13	0.05	—	—	—	25	149
	2-TC(1)	0.46	6.23	2.15	0.06	NA	13	134
	2-TC(2)	0.14	0.13	0.30	0.21	1.44	24	149
F	1-TC	0.05	0.09	—	—	—	51	190
	2-TC(1)	0.05	0.10	0.02	1.61	0.01	51	194
	2-TC(2)	0.05	0.21	2.58	2.10	1.23	51	192
G	1-TC	0.04	0.06	—	—	—	25	180
	2-TC(1)	0.04	0.05	0.00	0.14	0.02	25	184
	2-TC(2)	0.04	0.15	3.06	1.71	1.79	25	182
H	1-TC	0.12	0.07	—	—	—	18	151
	2-TC(1)	0.38	5.03	1.97	0.09	NA	9	133
	2-TC(2)	0.14	0.18	0.27	0.20	1.36	16	149
I	1-TC	0.03	0.08	—	—	—	19	184
	2-TC(1)	0.03	0.08	0.00	7.99	0.00	19	188
	2-TC(2)	0.03	0.17	2.04	1.73	1.18	19	186
J	1-TC	0.02	0.07	—	—	—	44	187
	2-TC(1)	0.02	0.07	0.00	0.00	0.02	44	191
	2-TC(2)	0.02	0.17	1.18	1.00	1.19	44	189

AIC, Akaike information criterion; BP_{ND}, binding potential; NA, not applicable ($k_3/k_4 > 20$); SS, residual sum of squares; 1-TC, one-tissue compartment model; 2-TC(1), unconstrained two-tissue compartment model; 2-TC(2), two-tissue compartment model with fixed K_1/k_2 ratio.

(E and H) the 2-TC(1) model significantly improved curve fitting in the cerebellar cortex. However, the kinetic parameters were not within a reasonable range.

Time–activity curves derived from target regions could be described with both the 1-TC and 2-TC(1) models showing no statistical preference for either of the models in the majority of subjects. Kinetic constants obtained in the prefrontal cortex, a large region with intermediate level of [^{11}C]AZ10419369 binding, are presented in Table 1. Findings in other regions were largely in agreement with those obtained for the prefrontal cortex. The 2-TC(1) model was statistically superior compared with the 1-TC model in 1 out of 10 subjects in the pallidum, temporal cortex, thalamus, and ventral striatum; in two subjects in the caudate nucleus, prefrontal cortex, and putamen; and in four subjects in the occipital cortex. However, although the 2-TC(1) model converged, reasonable estimates of the rate constants and the BP_{ND} (k_3/k_4) were not delivered with this model (Table 1).

In the next step of the kinetic modeling a variant of the 2-TC model was evaluated with K_1/k_2 constrained to the distribution volume obtained with the 1-TC model in the cerebellar cortex (2-TC(2)). Using this approach, estimates of BP_{ND} (k_3/k_4) were in a reasonable range in 9 out of 10 subjects (Table 1). However, valid estimates of the kinetic parameters could not be obtained for subject D because of the previously mentioned marked increase in radioactivity concentrations in plasma at the end of measurement. For this reason, subject D was considered as an outlier and data for this subject were not included in the comparison between the models. A representative graph of experimental data and curve fits obtained with the three different compartment models is presented in Figure 3C.

In the Logan graphical analysis with arterial input a linear phase was observed from 21 minutes for all regions, except for the pallidum, where a linear phase was observed after approximately 51 minutes (Figure 4). Estimates of V_T obtained with the linear graphical analysis were similar to values obtained with kinetic modeling, although slightly lower V_T values were obtained with the linear graphical method in the pallidum (Table 2). V_T values obtained with the 1-TC and 2-TC(2) models were correlated, at a statistically significant level, with values calculated using the Logan linear graphical analysis (Pearson's $r > 0.99$, $P < 0.0001$).

The next approach was to use cerebellar cortex as a reference region in the Logan reference tissue linear graphical analysis and in the SRTM. BP_{ND} values

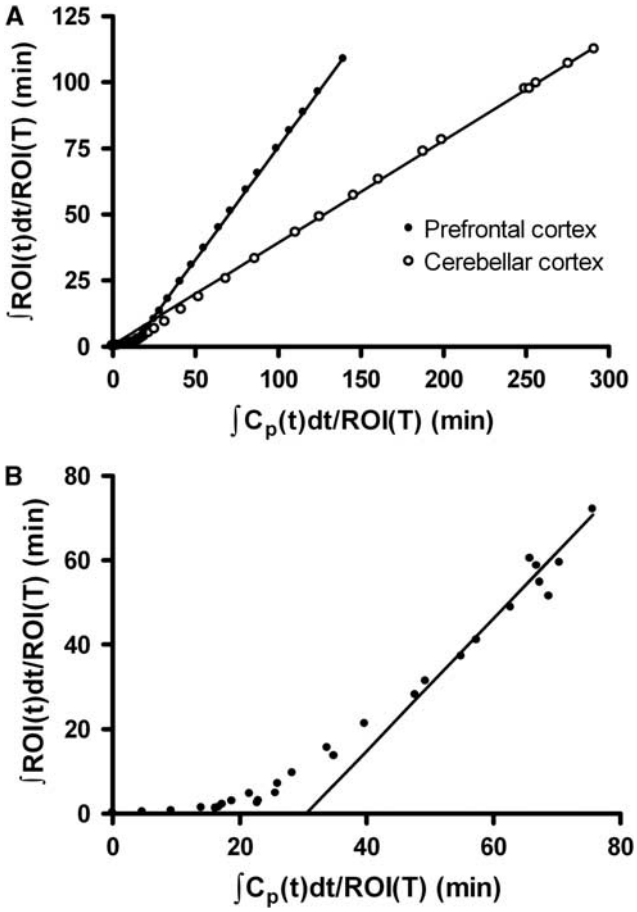

Figure 4 Linear graphical analysis of [^{11}C]AZ10419369 binding in the prefrontal cortex and cerebellar cortex (**A**) and pallidum (**B**) of subject C. ROI, radioactivity concentration in region of interest; Cp, plasma radioactivity concentration.

obtained with the Logan reference tissue method were in close correlation with those calculated based on V_T values obtained with the Logan graphical analysis with arterial input. BP_{ND} estimates obtained with reference tissue models showed a good correlation with BP_{ND} (k_3/k_4) values derived from the kinetic modeling, although the reference methods yielded on average 15% to 17% lower estimates (Table 2).

In a cross-validation approach correlations between BP_{ND} values calculated with four different methods (Table 2) were analyzed. BP_{ND} (k_3/k_4) values obtained with the 2-TC(2) model were correlated, at a statistically significant level, to BP_{ND} values calculated with Logan linear graphical approaches ($r > 0.90$, $P < 0.0001$), and with BP_{ND} values obtained with the SRTM ($r = 0.948$, $P < 0.0001$), although BP_{ND} values obtained with reference methods were underestimated compared with values obtained with the 2-TC(2) model (Supplementary Table S2). Regression slopes of corresponding linear relationships were 0.845 for the SRTM and 0.735 and 0.703 for the Logan linear graphical invasive and reference tissue methods, respectively.

When data for all regions were considered the correlation coefficients between BP_{ND} values obtained with the SRTM and the Logan invasive and reference methods were 0.969 and 0.933 ($P < 0.0001$), and regression slopes were 0.862 and 0.817 for the Logan invasive and Logan reference method, respectively. When data for the pallidum were excluded from the analysis, the agreement between BP_{ND} values obtained with SRTM and Logan invasive and reference methods was excellent with regression slopes close to unity (1.006 and 1.009, respectively; $r > 0.99$, $P < 0.0001$).

Table 2 Total volumes of distribution obtained by the 1-TC and 2-TC(2) models, and Logan linear graphical analysis with arterial input function, and binding potential values obtained with the 2-TC(2) model, Logan linear graphical analysis, and the simplified reference tissue model

Brain region		*Total volume of distribution, V_T (mL/cm^3)*			*Binding potential, BP_{ND}*			
		1-TC	*2-TC(2)*	*Logan*	*2-TC(2)*	*Logan*	*Logan ref*	*SRTM*
Pallidum	Mean (s.d.)	1.45 (1.04)	1.52 (1.08)	1.37 (0.96)	2.56 (0.74)	1.96 (0.59)	1.94 (0.53)	2.28 (0.61)
	COV	72%	71%	70%	29%	30%	27%	27%
Ventral striatum	Mean (s.d.)	1.32 (1.08)	1.33 (1.10)	1.31 (1.11)	1.95 (0.37)	1.70 (0.34)	1.70 (0.33)	1.68 (0.31)
	COV	82%	82%	84%	19%	20%	19%	18%
Occipital cortex	Mean (s.d.)	1.08 (0.85)	1.10 (0.87)	1.07 (0.83)	1.48 (0.25)	1.27 (0.20)	1.26 (0.21)	1.29 (0.20)
	COV	78%	79%	78%	17%	16%	17%	16%
Prefrontal cortex	Mean (s.d.)	1.00 (0.79)	1.01 (0.80)	0.99 (0.78)	1.32 (0.22)	1.13 (0.15)	1.13 (0.14)	1.12 (0.16)
	COV	78%	79%	78%	17%	13%	13%	14%
Putamen	Mean (s.d.)	0.97 (0.81)	0.99 (0.83)	0.96 (0.80)	1.17 (0.25)	0.99 (0.18)	0.99 (0.18)	0.97 (0.19)
	COV	84%	84%	83%	22%	18%	18%	19%
Caudate nucleus	Mean (s.d.)	0.91 (0.74)	0.92 (0.76)	0.90 (0.73)	1.07 (0.22)	0.90 (0.14)	0.89 (0.14)	0.89 (0.15)
	COV	81%	82%	81%	20%	15%	16%	17%
Temporal cortex	Mean (s.d.)	0.85 (0.63)	0.86 (0.64)	0.85 (0.62)	0.99 (0.15)	0.86 (0.14)	0.87 (0.14)	0.88 (0.16)
	COV	74%	75%	74%	15%	16%	16%	18%
Thalamus	Mean (s.d.)	0.59 (0.45)	0.62 (0.47)	0.61 (0.45)	0.41 (0.12)	0.31 (0.08)	0.30 (0.09)	0.31 (0.08)
	COV	76%	76%	75%	29%	26%	29%	27%
Cerebellar cortex	Mean (s.d.)	0.43 (0.33)		0.46 (0.35)				
	COV	75%		77%				

Logan, Logan linear graphical analysis with arterial input; Logan ref, Logan linear graphical analysis with reference tissue; SRTM, simplified reference tissue model; 1-TC, one-tissue compartment model; 2-TC(2), two-tissue compartment model with fixed K_1/k_2 ratio.
Values are presented as mean (s.d.) and percent coefficient of variation (COV); $n = 9$.

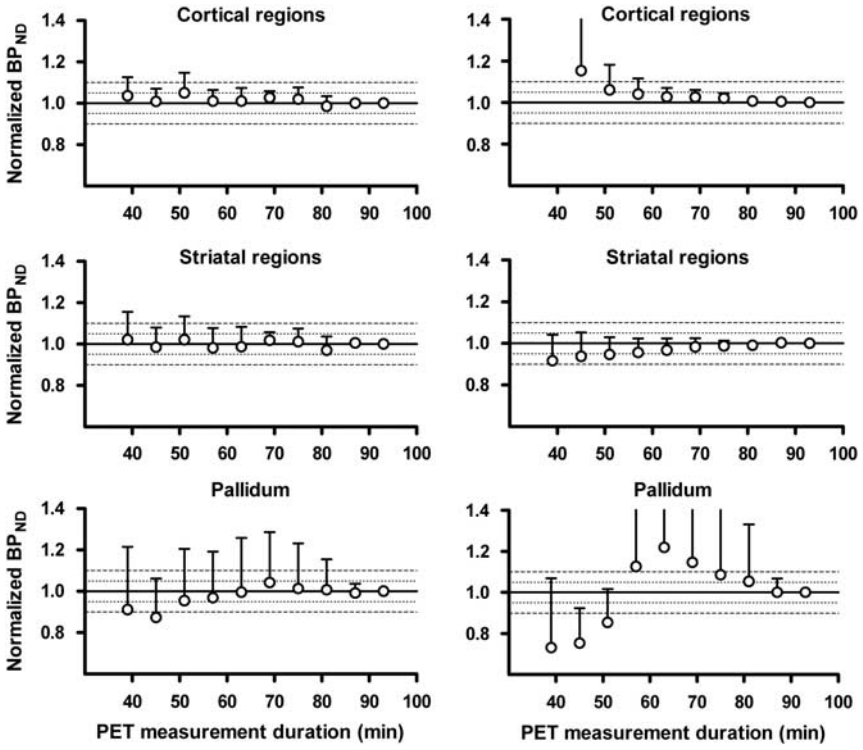

Figure 5 Time stability of [^{11}C]AZ10419369 binding potential (BP_{ND}) values obtained by the 2-TC(2) model (left panel) and the simplified reference tissue model (SRTM; right panel). BP_{ND} values are expressed relative to values obtained with a 93-minute positron emission tomography (PET) measurement. Data points and error bars represent mean and s.d., respectively.

To evaluate the time stability of V_T and BP_{ND} values obtained with kinetic modeling and the SRTM the effect of PET measurement duration on parameter estimates was analyzed. Time–activity curves for cerebellar cortex, cortical and striatal regions, and the pallidum were analyzed using the 1-TC and 2-TC(2) models and the SRTM using different measurement durations ranging from 39 to 87 minutes. Owing to low counting statistics, reasonable estimates of BP_{ND} in thalamus could not be obtained for measurement durations shorter than 93 minutes in subject J. Time–activity curves for this region were therefore not included in the analysis.

For all the measurement durations evaluated, V_T estimates obtained in the cortical regions and the cerebellar cortex were stable (90% $< V_T <$ 110%; s.d. $<$10%; Supplementary Figure S1). Mean estimates of V_T in striatal regions and pallidum were within $\pm$10% of the corresponding 93-minutes value for all measurement durations although s.d. was between 10% and 20% for durations shorter than 51 and 87 minutes, respectively (Supplementary Figure S1).

For cortical and striatal regions, estimates of BP_{ND} obtained by the 2-TC(2) model and the SRTM were stable for measurement durations longer than 51 minutes (Figure 5). BP_{ND} values obtained with these quantification methods in the pallidum met the criteria for stability for measurement durations longer than 81 minutes (Figure 5).

Discussion

In this study the binding of the novel 5-HT$_{1B}$ receptor radioligand, [^{11}C]AZ10419369, was examined in human subjects. BP_{ND} values were obtained using four different quantitative approaches, two based on arterial input function, and two based on reference tissue methods. For cross-validation purposes BP_{ND} values obtained with the four approaches were compared. In general, there was a good correlation between results obtained with the different quantitative models. The rank order of regional BP_{ND} values was the same and the coefficient of variation was similar for all methods. BP_{ND} values obtained with reference tissue models were in general well correlated to corresponding values obtained with kinetic modeling.

Binding of [^{11}C]AZ10419369 was highest in the pallidum, ventral striatum, and occipital cortex, followed by lower binding in the prefrontal cortex, dorsal striatum, and temporal cortex. Low concentrations were observed in the thalamus and cerebellar cortex. The rank order of regional radioactivity is thus in close agreement with the brain distribution of 5-HT$_{1B}$ receptors reported in autoradiographic studies (Bonaventure *et al*, 1997; Varnäs *et al*, 2001).

All subjects participated in the study according to the protocol. However, when analyzing the data it was observed that for one of the subjects (subject D) radioactivity in blood and plasma increased toward

the end of the measurement. The divergent shape of the blood radioactivity curve is unlikely to be explained by procedures involved with blood sampling or blood and plasma radioactivity measurements, as increasing radioactivity was observed also for an image-derived carotid artery time–activity curve (Figure 1B). The reason for this aberrant shape of the blood and plasma curve in one subject is not clear, but may have resulted from extravascular administration of a fraction of the radioligand injected. Such an explanation would be consistent with the later time of maximum brain radioactivity observed for this subject. Owing to the aberrant kinetics of the plasma curve, this subject was considered as an outlier and was not included in the subsequent comparison of models.

The cerebellar cortex was used as a reference region for nondisplaceable [^{11}C]AZ10419369 binding because the density of 5-HT$_{1B}$ receptors in this region has been suggested to be negligible based on results from autoradiographic studies (Varnäs *et al*, 2001, 2004). The absence of specific binding of [^{11}C]AZ10419369 in the cerebellar cortex has also been supported by observations from PET studies in macaques (Pierson *et al*, 2008) and *ex vivo* autoradiography studies of the guinea pig brain (Maier *et al*, 2009). In these studies, pretreatment with 5-HT$_{1B}$ receptor antagonists dose dependently reduced radioactivity in target regions, but not in the cerebellum. In the present kinetic modeling analysis of [^{11}C]AZ10419369 binding, there was no statistically significant improvement when using the 2-TC(1) instead of the 1-TC model for the cerebellar cortex in 8 of 10 subjects. This observation supports the model assumption of the 2-TC model as well as the SRTM, i.e., the free and nonspecific compartments equilibrate rapidly in the reference region, and can be combined into one single compartment corresponding to the nondisplaceable radioligand concentration (Huang *et al*, 1986; Lammertsma and Hume, 1996).

The compartmental analysis of [^{11}C]AZ10419369 data was based on a metabolite-corrected arterial input function. However, no significant amounts of radioactive metabolites were identified during the time of PET measurement in any of the 10 subjects analyzed. The absence of identifiable metabolites is in contrast to that previously found in a PET study with [^{11}C]AZ10419369 in macaques, wherein a metabolite fraction corresponding to 26% of the plasma radioactivity was observed 30 minutes after injection (Pierson *et al*, 2008). The low rate of metabolism is consistent with the slower decline of [^{11}C]AZ10419369 concentration in the brain tissue in humans as compared with macaques (Pierson *et al*, 2008). The absence of metabolites during the time of PET examination may be considered an advantage for radioligands as lipophilic metabolites may enter the brain and contribute to the measured signal.

In all regions, except for the pallidum the curves for specific binding, defined as the difference between radioactivity in target regions and radioactivity in cerebellar cortex, reached maximum values within time of PET data acquisition. This observation suggests that transient equilibrium was reached during the time of data acquisition. In the pallidum, slow binding kinetics has also been observed for the 5-HT$_{1B}$ receptor PET radioligand [^{11}C]P943, which does not reach equilibrium even after 120 minutes of measurement (Gallezot *et al*, 2010). As shown earlier for the very high-affinity radioligand [^{11}C]FLB457, the time required to reach equilibrium may be longer in regions having high receptor density (Olsson and Farde, 2001). One explanation for the late time of transient equilibrium in the pallidum may thus be the high 5-HT$_{1B}$ receptor density in this region. The late time of transient equilibrium of [^{11}C]AZ10419369 in the pallidum suggests that longer PET acquisition times may be required for quantification of 5-HT$_{1B}$ receptor binding in this region.

The unconstrained 2-TC model could not describe 5-HT$_{1B}$ receptor binding in a reasonable manner in all subjects. Although the model converged, estimates of the rate constants and the k_3/k_4 ratio were highly variable and not reasonable (above 1). The next approach was to constrain the K_1/k_2 ratio to the distribution volume in the cerebellar cortex (2-TC(2) model). Although estimates of individual rate constants were highly variable even using this approach, reasonable estimates of V_T and BP_{ND} were obtained.

When applying the Logan linear graphical analysis a linear phase was observed in most regions. However, because of slow binding kinetics the linear phase was reached only at late time points for the pallidum. For this reason, the Logan linear graphical method may underestimate V_T for this region. Consequently, lower V_T values were observed in this region when compared with the corresponding values obtained with the 1-TC and 2-TC(2) models.

There was a high interindividual variability in V_T (see Table 2). This could be explained by a 10-fold variation in plasma radioactivity concentration between the subjects. However, brain radioactivity and regional BP_{ND} values did not show such high interindividual variability, indicating a similar free concentration in plasma between the subjects. The variation in plasma concentration and V_T values may thus be due to interindividual differences in plasma protein binding. However, plasma protein binding of [^{11}C]AZ10419369 was not examined in this study.

Reference tissue models used for neuroreceptor quantification offer advantages by avoiding the need for arterial blood sampling. The suitability of reference tissue models for the analysis of [^{11}C]AZ10419369 binding was therefore explored. Two reference tissue approaches were evaluated, the Logan linear graphical reference tissue method and the SRTM. BP_{ND} values obtained with the Logan reference tissue model were in close agreement with those calculated with the Logan invasive method. BP_{ND} values in the pallidum were thus lower than

BP_{ND} values obtained with kinetic modeling because of the late time of transient equilibrium in this region. The SRTM may offer advantages in regions of late equilibrium as it considers the entire time–activity curve. The SRTM provided BP_{ND} values consistent with values obtained with kinetic modeling for all regions, including the pallidum. On the basis of the good correlation between BP_{ND} values obtained with the SRTM and kinetic modeling, we propose that the SRTM is the most suitable method for applied clinical studies.

During the course of this study the characterization of another 5-HT_{1B} receptor PET radioligand, [^{11}C]P943, has been reported in the literature (Gallezot *et al*, 2010). The rank of regional BP_{ND} values obtained with [^{11}C]AZ10419369 is in good correspondence to those reported for [^{11}C]P943, although BP_{ND} values obtained with [^{11}C]AZ10419369 are approximately 30% to 40% higher. These differences may reflect differences in kinetic behavior between the two radioligands. For a detailed comparison between the binding characteristics of the two tracers, a direct comparison study in the same subjects is needed.

Conclusions

[^{11}C]AZ10419369 binding to central 5-HT_{1B} receptors in human subjects can be described by classic compartmental models. BP_{ND} values obtained with kinetic compartment analysis and simplified models using the cerebellar cortex as reference region were well correlated. However, because of the late time of equilibrium in the pallidum, longer times of PET acquisition may be required for quantification of [^{11}C]AZ10419369 binding in this region. Noninvasive quantitative methods may be applied in future studies evaluating drug-induced receptor occupancy and measurement of brain 5-HT_{1B} receptor levels in patients with psychiatric disorders.

Acknowledgements

The authors thank all members of the PET group at the Karolinska Institutet for their kind assistance during this study.

Conflict of interest

This work was funded by AstraZeneca Pharmaceuticals. Six of the authors are employees at AstraZeneca Pharmaceuticals.

References

Åhlander-Lüttgen M, Madjid N, Schött PA, Sandin J, Ögren SO (2003) Analysis of the role of the 5-HT_{1B} receptor in spatial and aversive learning in the rat. *Neuropsychopharmacology* 28:1642–55

Akaike H (1974) A new look at the statistical model identification. *IEEE Trans Automat Contr* 19:716–23

Barnes NM, Sharp T (1999) A review of central 5-HT receptors and their function. *Neuropharmacology* 38:1083–152

Bonaventure P, Schotte A, Cras P, Leysen JE (1997) Autoradiographic mapping of 5-HT_{1B}- and 5-HT_{1D} receptors in human brain using [^{3}H]alniditan, a new radioligand. *Receptors Channels* 5:225–30

Crabbe JC, Phillips TJ, Feller DJ, Hen R, Wenger CD, Lessov CN, Schafer GL (1996) Elevated alcohol consumption in null mutant mice lacking 5-HT_{1B} serotonin receptors. *Nat Genet* 14:98–101

Engel G, Göthert M, Hoyer D, Schlicker E, Hillenbrand K (1986) Identity of inhibitory presynaptic 5-hydroxytryptamine (5-HT) autoreceptors in the rat brain cortex with 5-HT_{1B} binding sites. *Naunyn Schmiedebergs Arch Pharmacol* 332:1–7

Eriksson L, Holte S, Bohm C, Kesselberg M, Hovander B (1988) Automated blood sampling systems for positron emission tomography. *IEEE Trans Nucl Sci* 35:703–7

Farde L, Eriksson L, Blomquist G, Halldin C (1989) Kinetic analysis of central [^{11}C]raclopride binding to D_2-dopamine receptors studied by PET–a comparison to the equilibrium analysis. *J Cereb Blood Flow Metab* 9:696–708

Gallezot JD, Nabulsi N, Neumeister A, Planeta-Wilson B, Williams WA, Singhal T, Kim S, Maguire RP, McCarthy T, Frost JJ, Huang Y, Ding YS, Carson RE (2010) Kinetic modeling of the serotonin 5-HT_{1B} receptor radioligand [^{11}C]P943 in humans. *J Cereb Blood Flow Metab* 30:196–210

Gingrich JA, Hen R (2001) Dissecting the role of the serotonin system in neuropsychiatric disorders using knockout mice. *Psychopharmacology (Berl)* 155:1–10

Halldin C, Swahn CG, Farde L, Sedvall G (1995) Radioligand disposition and metabolism. In: *PET for drug development and evaluation* (Comar D, ed), Kluwer Academic Publishers: Dordrecht, The Netherlands, 55–65

Hoyer D, Hannon JP, Martin GR (2002) Molecular, pharmacological and functional diversity of 5-HT receptors. *Pharmacol Biochem Behav* 71:533–54

Huang SC, Barrio JR, Phelps ME (1986) Neuroreceptor assay with positron emission tomography: equilibrium versus dynamic approaches. *J Cereb Blood Flow Metab* 6:515–21

Innis RB, Cunningham VJ, Delforge J, Fujita M, Gjedde A, Gunn RN, Holden J, Houle S, Huang SC, Ichise M, Iida H, Ito H, Kimura Y, Koeppe RA, Knudsen GM, Knuuti J, Lammertsma AA, Laruelle M, Logan J, Maguire RP, Mintun MA, Morris ED, Parsey R, Price JC, Slifstein M, Sossi V, Suhara T, Votaw JR, Wong DF, Carson RE (2007) Consensus nomenclature for *in vivo* imaging of reversibly binding radioligands. *J Cereb Blood Flow Metab* 27:1533–9

Lammertsma AA, Hume SP (1996) Simplified reference tissue model for PET receptor studies. *Neuroimage* 4:153–8

Lee MD, Simansky KJ (1997) CP-94, 253: a selective serotonin1B (5-HT_{1B}) agonist thatpromotes satiety. *Psychopharmacology (Berl)* 131:264–70

Leenders KL, Perani D, Lammertsma AA, Heather JD, Buckingham P, Healy MJ, Gibbs JM, Wise RJ, Hatazawa J, Herold S, Beaney RP, Brooks DJ, Spinks T, Rhodes C, Frackowiak RSJ, Jones T (1990) Cerebral blood flow, blood volume and oxygen utilization. Normalvalues and effect of age. *Brain* 113:27–47

Lin D, Parsons LH (2002) Anxiogenic-like effect of serotonin$_{1B}$ receptor stimulation in the rat elevated plus-maze. *Pharmacol Biochem Behav* 71:581–7

Logan J, Fowler JS, Volkow ND, Wang GJ, Ding YS, Alexoff DL (1996) Distribution volume ratios without blood sampling from graphical analysis of PET data. *J Cereb Blood Flow Metab* 16:834–40

Logan J, Fowler JS, Volkow ND, Wolf AP, Dewey SL, Schlyer DJ, MacGregor RR, Hitzemann R, Bendriem B, Gatley SJ, Christman DR (1990) Graphical analysis of reversible radioligand binding from time-activity measurements applied to [*N*-^{11}C-methyl]-(-)-cocaine PET studies in human subjects. *J Cereb Blood Flow Metab* 10:740–7

Maier DL, Sobotka-Briner C, Ding M, Powell ME, Jiang Q, Hill G, Heys JR, Elmore CS, Pierson ME, Mrzljak L (2009) [N-methyl-$^3H_3$]AZ10419369 binding to the 5-HT_{1B} receptor: *in vitro* characterization and *in vivo* receptor occupancy. *J Pharmacol Exp Ther* 330:342–51

Malleret G, Hen R, Guillou JL, Segu L, Buhot MC (1999) 5-HT_{1B} receptor knock-out mice exhibit increased exploratory activity and enhanced spatial memory performance in the Morris water maze. *J Neurosci* 19:6157–68

Maura G, Raiteri M (1986) Cholinergic terminals in rat hippocampus possess 5-HT_{1B} receptors mediating inhibition of acetylcholine release. *Eur J Pharmacol* 129:333–7

Mawlawi O, Martinez D, Slifstein M, Broft A, Chatterjee R, Hwang DR, Huang Y, Simpson N, Ngo K, Van Heertum R, Laruelle M (2001) Imaging human mesolimbic dopamine transmission with positron emission tomography: I. Accuracy and precision of D_2 receptor parameter measurements in ventral striatum. *J Cereb Blood Flow Metab* 21:1034–57

Mintun MA, Raichle ME, Kilbourn MR, Wooten GF, Welch MJ (1984) A quantitative model for the *in vivo* assessment of drug binding sites with positron emission tomography. *Ann Neurol* 15:217–27

Olsson H, Farde L (2001) Potentials and pitfalls using high affinity radioligands in PET and SPET determinations on regional drug induced D2 receptor occupancy—a simulation study based on experimental data. *Neuroimage* 14:936–45

Pierson ME, Andersson J, Nyberg S, McCarthy DJ, Finnema SJ, Varnäs K, Takano A, Karlsson P, Gulyás B, Medd AM, Lee CM, Powell ME, Heys JR, Potts W, Seneca N, Mrzljak L, Farde L, Halldin C (2008) [^{11}C]AZ10419369: A selective 5-HT_{1B} receptor radioligand suitable for positron emission tomography (PET). Characterization in the primate brain. *Neuroimage* 41:1075–85

Ramboz S, Saudou F, Amara DA, Belzung C, Segu L, Misslin R, Buhot MC, Hen R (1996) 5-HT_{1B} receptor knock out—behavioral consequences. *Behav Brain Res* 73:305–12

Rocha BA, Scearce-Levie K, Lucas JJ, Hiroi N, Castanon N, Crabbe JC, Nestler EJ, Hen R (1998) Increased vulnerability to cocaine in mice lacking the serotonin-1B receptor. *Nature* 393:175–8

Roland PE, Graufelds CJ, Wåhlin L, Ingelman L, Andersson M, Ledberg A, Pedersen J, Åkerman S, Dabringhaus A, Zilles K (1994) Human Brain Atlas: for high-resolution functional and anatomical mapping. *Hum Brain Mapp* 1:173–84

Ruf BM, Bhagwagar Z (2009) The 5-HT_{1B} receptor: a novel target for the pathophysiology of depression. *Curr Drug Targets* 10:1118–38

Sarhan H, Grimaldi B, Hen R, Fillion G (2000) 5-HT_{1B} receptors modulate release of [^{3}H]dopamine from rat striatal synaptosomes: further evidence using 5-HT moduline, polyclonal 5-HT_{1B} receptor antibodies and 5-HT_{1B} receptor knock-out mice. *Naunyn Schmiedebergs Arch Pharmacol* 361:12–8

Sari Y, Miquel MC, Brisorgueil MJ, Ruiz G, Doucet E, Hamon M, Vergé D (1999) Cellular and subcellular localization of 5-hydroxytryptamine1B receptors in the rat central nervous system: immunocytochemical, autoradiographic and lesion studies. *Neuroscience* 88:899–915

Saudou F, Amara DA, Dierich A, LeMeur M, Ramboz S, Segu L, Buhot MC, Hen R (1994) Enhanced aggressive behavior in mice lacking 5-HT_{1B} receptor. *Science* 265:1875–8

Svarer C, Madsen K, Hasselbalch SG, Pinborg LH, Haugbøl S, Frøkjær VG, Holm S, Paulson OB, Knudsen GM (2005) MR-based automatic delineation of volumes of interest in human brain PET images using probability maps. *Neuroimage* 24:969–79

Varnäs K, Hall H, Bonaventure P, Sedvall G (2001) Autoradiographic mapping of 5-HT_{1B} and 5-HT_{1D} receptors in the postmortem human brain using [^{3}H]GR 125743. *Brain Res* 915:47–57

Varnäs K, Halldin C, Hall H (2004) Autoradiographic distribution of serotonin transporters and receptor subtypes in human brain. *Hum Brain Mapp* 22:246–60

Wienhard K, Dahlbom M, Eriksson L, Michel C, Bruckbauer T, Pietrzyk U, Heiss WD (1994) The ECAT EXACT HR: performance of a new high resolution positron scanner. *J Comput Assist Tomogr* 18:110–8

Wong DF, Gjedde A, Wagner Jr HN (1986) Quantification of neuroreceptors in the living human brain. I. Irreversible binding of ligands. *J Cereb Blood Flow Metab* 6:137–46

Supplementary Information accompanies the paper on the Journal of Cerebral Blood Flow & Metabolism website (http://www.nature.com/jcbfm)